Intersite Coulomb Interactions in Charge-Ordered Systems

Bo Gyu Jang,[1,*] Minjae Kim,[1,†] Sang-Hoon Lee,[1] Wooil Yang,[2,1] Seung-Hoon Jhi,[2] and Young-Woo Son[1,‡]
[1]Korea Institute for Advanced Study, Seoul 02455, Republic of Korea
[2]Department of Physics, Pohang University of Science and Technology, Pohang 37673, Republic of Korea

(Received 5 May 2022; revised 17 August 2022; accepted 16 March 2023; published 28 March 2023)

Using *ab initio* approaches for extended Hubbard interactions coupled to phonons, we reveal that the intersite Coulomb interaction plays important roles in determining various distinctive phases of the paradigmatic charge-ordered materials of $Ba_{1-x}K_xAO_3$ (A = Bi and Sb). We demonstrated that all their salient doping dependent experiment features such as breathing instabilities, anomalous phonon dispersions, and transition between charge-density wave and superconducting states can be accounted for very well if self-consistently obtained nearest neighbor Hubbard interactions are included, thus establishing a minimal criterion for reliable descriptions of spontaneous charge orders in solids.

DOI: 10.1103/PhysRevLett.130.136401

Since Verwey found the metal-to-insulator transition (MIT) in magnetite (Fe_3O_4) owing to long-range order of alternating Fe^{2+} and Fe^{3+} ions [1], the charge-ordered state has been one of the central issues in condensed matter physics. It often occurs near MITs, superconducting (SC), or charge density wave (CDW) states [2–9]. This local charge ordering (CO) can lead to colossal magnetoresistance, ferroelectricity, or multiferroicity [10,11]. In addition, the CO in high-temperature cuprate superconductors has also been studied intensively to understand its roles as a leading competitor of SC state [4–7].

Charge-ordered materials host atoms with disparate charging states that are closely placed, invoking the strong Coulomb interactions and distorting lattices to relieve their energetic cost [12]. Hence, theories for the systems should treat the interaction as well as its coupling to lattices on an equal footing. Typical approaches based on density functional theory with the local density approximation (DFT-LDA) [13] or generalized gradient approximation (GGA) [14] fail to describe their properties [15,16]. The addition of on-site Hubbard interaction (U) within DFT (DFT + U) [17,18] captures a correct CO state when the intersite interaction is screened [15]. Except for a few cases, however, it is insufficient in obtaining the ground states [19–21]. Therefore, advanced methods beyond the local corrections are needed to figure the role of the interactions in COs.

Perovskite $BaBiO_3$ (BBO) and $BaSbO_3$ (BSO) are prototypical CO materials that are not well understood by DFT-GGA and DFT + U [22–34]. They show CDW states characterized by breathing distortion of oxygen octahedra with the charge disproportionations of Bi ions [22–24]. The CDW is suppressed by substituting Ba with K and the SC phase occurs at a relatively higher transition temperature (T_c) [8,9]. A few recent studies based on the Heyd-Scuseria-Ernzerhof (HSE) hybrid functional and GW approximation (GWA) can capture the insulating ground state of BBO and obtain enhanced electron-phonon ($e-ph$) interactions, providing a clue to understanding the observed T_c [31–35]. However, realistic full phonon spectra to understand the transition between SC and CDW states for experimentally accessible doping levels are hardly available due to demanding computational resources and computed frequency is usually overestimated for strongly coupled phonons [26,33,34].

On the other hand, recent developments on self-consistent evaluations of U [36,37] and intersite Hubbard interactions (V) [38,39] within DFT (DFT + U + V) [40] successfully describe various properties of solids [38–49]. Owing to their low computational cost comparable to DFT-LDA and improved accuracy to GWA [38,46], the new method provides an opportunity to study the correlated solids in large scale structures and full phase space of interests. Motivated by these developments as well as the works on BBO and BSO, we have carried out *ab initio* study to explore the role of the interactions for interplay between their electronic and structural properties.

In this Letter, we theoretically demonstrate that the evolution of charge-ordered states in bismuthates and antimonates with potassium doping is essentially controlled by the doping-dependent nonlocal Coulomb interaction. Our new parameter-free *ab initio* method for extended Hubbard interactions [38,46] can compute electronic energy bands as well as full phonon dispersions of $Ba_{1-x}K_xAO_3$ (A = Bi and Sb) for the whole phase space with structural phase transitions, agreeing well with all the key measurements only when intersite Coulomb interactions are included. Our establishments imply that the explicit treatment of the nonlocal interactions is critical for the description of the intertwined charge and lattice degrees of freedom in charge-ordered materials.

Our DFT $+ U + V$ method uses the total energy functional of $E_{\rm tot} = E_{\rm DFT} + E_{\rm Hub}$ that can be decomposed into (semi) local density functional of $E_{\rm DFT}$ and Hubbard functional with double counting corrections [40], $E_{\rm Hub} = \frac{1}{2}\sum_I U_I \times \sum_{m,m',\sigma}(\delta_{mm'} - n^{II\sigma}_{mm'})n^{II\sigma}_{m'm} - \frac{1}{2}\sum_{\{I,J\}} V_{IJ}\sum_{m,m',\sigma} n^{IJ\sigma}_{mm'} n^{JI\sigma}_{m'm}$, where the generalized occupation matrix is $n^{IJ\sigma}_{mm'} = \sum_{\mathbf{k}\nu} f^{\sigma}_{\mathbf{k}\nu} \langle \psi^{\sigma}_{\mathbf{k}\nu}|\phi^{J}_{m'}\rangle \langle \phi^{I}_{m}|\psi^{\sigma}_{\mathbf{k}\nu}\rangle$, $f^{\sigma}_{\mathbf{k}\nu}$ the Fermi-Dirac function of Kohn-Sham orbital of $\psi^{\sigma}_{\mathbf{k}\nu}$ of the νth band with spin σ at momentum $\mathbf{k}$, and ϕ^{I}_{m} the localized orbitals with angular quantum number m. Here, I and J are abbreviated indexes for atomic positions and principal and azimuthal quantum numbers together and $\{I, J\}$ denotes a pair of atoms within the nearest neighboring distances. We obtain self-consistent U_I and V_{IJ} using new pseudohybrid functionals for Hubbard interactions [36–39]. We also consider rotationally invariant interactions [38,40] so that U and V for valence s and p orbitals of Bi (Sb) and $2p$ orbital of O are computed as shown in Table I. Detailed parameters are in Supplemental Material [50].

At low-temperature, BBO is the monoclinic structure having oxygen octahedra with breathing distortion of displacement by δ_B and a tilting angle of θ_T between them as shown in Fig. 1(a), while BSO has δ_B only, resulting in fcc structure ($Fm\bar{3}m$) [24]. We first investigate the artificial double-well potential induced by δ_B without tilting [Fig. 1(b)]. For BBO, our DFT-GGA calculation underestimates δ_B with a very shallow potential well [26,28]. The breathing distortion, however, is significantly enhanced in DFT $+ U + V$ calculation. Unlike BBO, BSO has a relatively deep potential with DFT-GGA. Nonetheless, the energy gain from the breathing distortion in BSO also becomes larger with the extended Hubbard interactions.

As shown in the model potential wells in Fig. 1(b), DFT $+$ $U + V$ well captures a part of CDW states of the undoped cases. Our results on a fully relaxed monoclinic BBO are summarized and compared with the previous studies (Table II). If tilting of θ_T is allowed, DFT-GGA accidentally reproduces δ_B owing to its overestimation of volume by ~4% and θ_T by ~14% but still cannot describe the insulating gap of the CDW state like a previous work [31]. On the other hand, DFT $+ U + V$ calculation well describes all the critical experimental parameters.

To investigate the effects of U and V in metallic BBO above the CDW transition temperature of 800 K, we compute the energy bands of BBO in the perfect cubic perovskite phase with experimental volume, using DFT-GGA, DFT $+ U + V$, and GWA as shown in Figs. 2(a) and 2(b). The width of the energy band crossing the Fermi level (E_F) is enhanced with both DFT $+ U + V$ and GWA compared with one with DFT-GGA. We also note that the DFT-GGA bands for fully occupied states associated with oxygen p orbitals shifted down by including U^O_p in the DFT $+ U + V$ and by the self-energy corrections in the GWA method.

Effects of intersite interaction are also conspicuous for electronic structures of the CDW state. Figure 2(c) shows the calculated density of states (DOS) of BBO with the fully relaxed monoclinic CDW structure obtained from each method (Table II) together with previous GWA results and photoemission spectroscopy (PES) data [58,59]. The two experiments show the quite different positions of the highest PES peak below E_F (−3 and −5 eV, respectively), that may originate from the different substrate

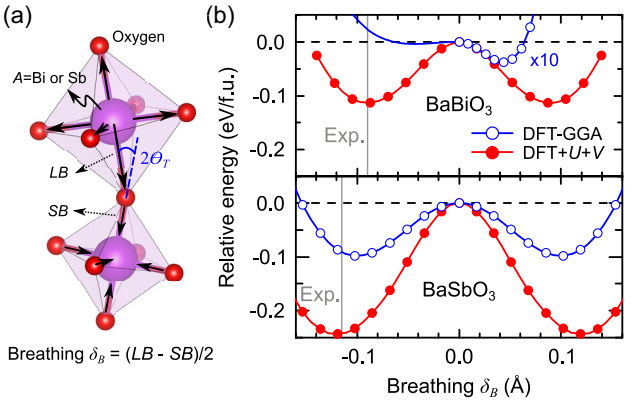

FIG. 1. (a) Atomic model for distorted octahedra in the CDW state of BB(S)O. Breathing distortion of δ_B and tilting angle of θ_T are defined as an averaged length difference between Bi(Sb)-O bonds and as an angle between vertical axes belonging to adjacent octahedra, respectively. (b) Double-well potential as a function of δ_B. Blue, red, and gray lines indicate DFT-GGA, DFT $+ U + V$, and experiments [24,56], respectively. The DFT-GGA results for $\delta_B > 0$ are enlarged by 10 times to show the minimum for breathing distortion clearly.

TABLE I. Calculated U and V (in eV) for BaAO_3 (A = Bi and Sb). $U^A_{s(p)}$ (U^O_p) are on-site Hubbard parameters of valence $s(p)$ orbital of $A(O)$ atom. $V_{sp(pp)}$ are the intersite Hubbard parameters between the $s(p)$ orbital of A and p orbital of O.

A	U^A_s	U^A_p	U^O_p	V_{sp}	V_{pp}
Bi	1.03	0.11	8.18	1.78	1.59
Sb	0.92	0.13	8.18	1.86	1.61

TABLE II. Calculated structural and electronic properties of BBO along with computational and experimental data from previous studies. v: volume, β: monoclinic angle, δ_B: breathing distortion, θ_T: tilting distortion, and E_g: band gap.

	Experiments[a]	HSE[b]	DFT-GGA	DFT $+ U + V$
v (Å^3)	81.80–82.54	82.10	85.03	82.94
β (deg)	90.16–90.27	90.24	90.39	90.34
δ_B (Å)	0.08–0.09	0.09	0.08	0.10
θ_T (°)	10.12–10.72	11.9	11.75	10.46
E_g (eV)	0.8–1.1	0.84	0.0	0.99

[a]References [22,56,57].
[b]Reference [31].

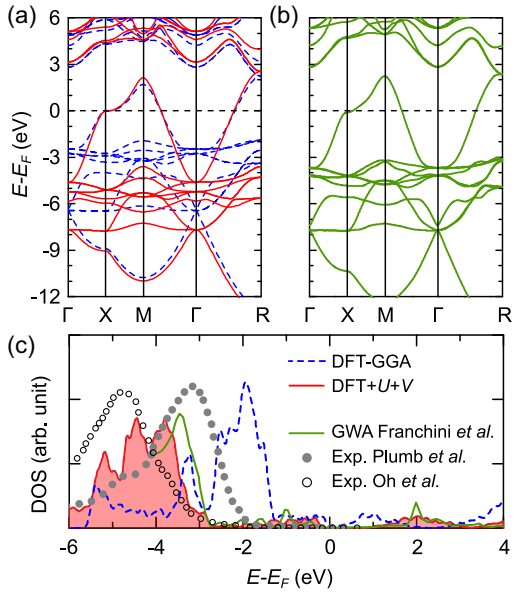

FIG. 2. Energy bands of BBO of cubic perovskite structure obtained from the (a) DFT (blue) and DFT + U + V (red) and (b) GWA method. Here we use GW_0 approximation for the GWA. (c) Density of states for monoclinic CDW structure. Blue, red, and green lines indicate DFT, DFT + U + V, and previous GWA results [31], respectively. Empty circles are from photoemission spectroscopy measurements [58,59].

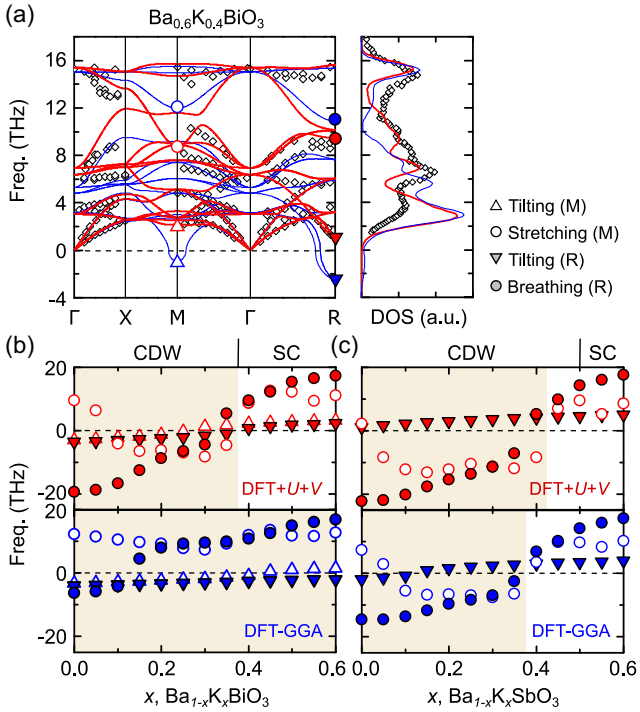

FIG. 3. (a) Phonon dispersion and DOS of $Ba_{0.6}K_{0.4}BiO_3$. Open diamonds and blue (red) lines indicate experiments [61,62] and the DFT-GGA (DFT + U + V) results, respectively. Frequencies of the four selected modes are marked by open and filled triangles and circles at the M and R points, respectively. Phonon frequency variations of the four modes as increasing K doping level in (b) BKBO and (c) BKSO. Top and bottom panels are for the modes obtained by DFT + U + V and DFT-GGA methods, respectively. Experimental [24,56], and our theoretical phase boundaries between the CDW and SC states are shown on the upper abscissa and denoted by background color changes in (b) and (c), respectively.

conditions [59]. As shown in Fig. 2(c), the DOS peak position for oxygen $2p$ orbitals from DFT-GGA is significantly off the experimental one. Furthermore, the energy gap of the CDW state is absent despite the correct δ_B. Unlike DFT-GGA results, the DOS using DFT + U + V well agrees with the experiments and the previous GWA calculation [31]. The O $2p$ peak position is located at around −4 eV, which is in between two experimental results. The band gap is about 1 eV, consistent with the experimental results. Although U_p^O is critical for the down-shifted bands for O $2p$ orbitals, we note that the DFT + U without V still substantially underestimates the CDW band gap (Table S1 in the Supplemental Material [50]).

The results so far demonstrate that our new method describes correctly the electronic and structural properties of undoped bismuthate and antimonates without serious computational costs. Thus, it enables the study of the nonlocal interaction effects on phonons with various K doping levels thoroughly, which could not be done with the HSE or GWA method easily. From now on, we present the comprehensive phonon dispersions using the frozen phonon techniques [60] with extended Hubbard interactions to examine the structural instability of potassium doped $Ba_{1-x}K_xBiO_3$ and $Ba_{1-x}K_xSbO_3$ (BKBO and BKSO). Related computational details are in the Supplemental Material [50].

Figure 3(a) shows the phonon dispersion and DOS of $Ba_{0.6}K_{0.4}BiO_3$ together with experimental data [61,62]. Here we focus on four representative phonon modes related with CDW states in BKBO and BKSO systems; stretching and in-phase tilting modes at the M point and breathing and antiphase titling modes at the R point. For the stretching mode, the Bi-O bond length changes along only two axes of the oxygen octahedron while it changes along all three axes in the breathing mode. In Fig. 3(a), it is immediately noticeable that the unstable in(anti)-phase tilting mode at the $M(R)$ point obtained by DFT-GGA hardens enough to be stable when V is included, agreeing with experiments. Not only low frequency modes, but the high frequency optical branches obtained with V also agree with experiments. Specifically, our result well matches the anomalous dispersion of the LO mode along ΓX [61,63,64] related with the instability toward the charge ordering [63,64].

We present doping-dependent evolution of frequencies for the selected phonon modes of BKBO and BSBO in Figs. 3(b) and 3(c). Our calculations with the extended Hubbard interactions fruitfully reflect the measured trends of structural distortions for the both systems. In the case of BKBO shown in Fig. 3(b), the breathing mode computed using DFT-GGA becomes to be stable when $x \geq 0.15$ while it does only when

$x \geq 0.4$ in the experiments [64–66] and our results with V. BKBO with $x \geq 0.4$ show SC states without structural distortions [9,56,61,67] while the tilting instabilities still remain in DFT-GGA as shown in Figs. 3(a) and 3(b) [34]. This is in sharp contrast to the complete absence of instability in the DFT + U + V results when $x \geq 0.4$. Thus, the nonlocal Coulomb interaction is decisive in capturing the transition between CDW and SC states of BKBO.

As already shown in Fig. 1(b), the effect of V is not as crucial in BKSO as it is in BKBO. Nevertheless, our method makes improvements in describing experimental phase diagram as shown in Fig. 3(c). For undoped cases, DFT-GGA shows the tilting instability in addition to the breathing instability while only the latter is observed in the experiment. Our calculation with V results in a perfect fcc structure [24]. In addition, the CDW phase survives up to higher doping of $x \simeq 0.4$ in the DFT + U + V calculation, which is closer to the experimental phase boundary of $x \simeq 0.5$, due to the enhanced stretching instability. Comprehensive comparisons between results from DFT + U and DFT + U + V and detailed discussions are in Sec. D, Figs. S2, S5, and S7 of the Supplemental Material [50].

Finally, we estimate the effects of nonlocal interactions on e-ph coupling constant (λ) for the breathing mode that is an important factor for the SC state. Instead of calculating λ explicitly, we compute "reduced e-ph matrix element" [30,33,68], $D^{\mu\mathbf{k}}_{\alpha\mathbf{q}} = \partial\epsilon_{\mu\mathbf{k}}/\partial\mathbf{u}^{\alpha}_{\mathbf{q}}$ to compare with previous studies based on HSE directly [33,35]. Here, $\mathbf{u}^{\alpha}_{\mathbf{q}}$ is a displacement vector of phonon mode α with the wavevector $\mathbf{q}$ and $\epsilon_{\mu\mathbf{k}}$ energy of μth band at $\mathbf{k}$. Specifically, following previous works [33,35], we obtain the reduced element of D^{L}_{R} for the energy band crossing the E_F at $\mathbf{k}$ of the L point by the breathing mode at $\mathbf{q}$ of the R point (see Fig. S3 in Supplemental Material [50]).

For both systems, D^{L}_{R} increases with doping within DFT-GGA and DFT + U as shown in Fig. 4. In sharp contrast to this, the matrix element with V decreases with increasing x for BKBO while it remains more or less the same for BKSO. So, the matrix element of the latter becomes larger than that of the former for $x > 0.3$. Considering that the coupling can be roughly estimated as $\lambda \sim (D^{\mu\mathbf{k}}_{\alpha\mathbf{q}}/\omega^{\alpha}_{\mathbf{q}})^2$ for phonon frequency $\omega^{\alpha}_{\mathbf{q}}$ [30,33,68], Fig. 4 implies a higher T_c of BKSO than BKBO at larger doping levels with V, agreeing with a recent experiment [24]. We also note that our estimations are consistent with two previous HSE results for a few selected dopings [33,35].

The opposite trends of D^{L}_{R}'s for different computational methods can be understood by considering intersite interactions under lattice distortions. The paired octahedra with the breathing modes in Fig. 1 have an elongated long bond (LB) and a shrinking short bond (SB) between Bi(Sb) and oxygens [24]. Based on a perturbation theory, D^{L}_{R} can be written as $D^{L}_{R}\delta u_B \simeq \varepsilon_{\mathrm{SB}} - \varepsilon_{\mathrm{LB}} - V(n_{\mathrm{SB}} - n_{\mathrm{LB}})$, where $\varepsilon_{\mathrm{SB(LB)}}$ and $n_{\mathrm{SB(LB)}}$ are the energy level and density matrix for SB(LB), respectively, and δu_B is the perturbation amplitude of the breathing mode (See Supplemental Material [50] for detailed derivations). Since $n_{\mathrm{LB}} > n_{\mathrm{SB}}$ for lower dopings, the intersite interaction should enhance the matrix elements over those from DFT-GGA and DFT + U. As doping level is increased, the difference between n_{LB} and n_{SB} diminishes so that the effect of nonlocal interactions vanishes as shown in Fig. 4, thus highlighting again a critical role of V for doping dependent electron-phonon interactions.

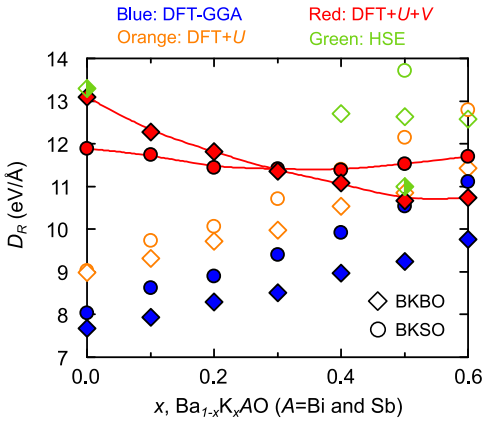

FIG. 4. Reduced e-ph matrix element (D^{L}_{R}) as a function of doping x. Diamonds (circles) denote BKB(S)O and blue, orange, and red color indicate DFT-GGA, DFT + U, and DFT + U + V results, respectively. Open and right-half diamonds are HSE results for the element from Refs. [35] and [33], respectively.

In summary, we present a comprehensive study on the doping dependent electronic and structural properties of prototypical charge-ordered materials, BKBO and BKSO using a newly developed *ab initio* computational method. We demonstrated that the nonlocal Coulomb interactions between the nearest neighbors are essential physical parameters in determining the doping dependent evolution of CDW and SC states, highlighting nontrivial relationships between the nonlocal interaction, charge order, and lattice distortion in correlated materials.

B. G. J., M. K., and W. Y. were supported by Korea Institute for Advanced Study (KIAS) individual Grants (No. QP081301, No. CG083501, No. QP090101). S.-H. J. was supported by NRF of Korea (Grant No. 2022R1A2C1006530) funded by the Korea government (MSIT). Y.-W. S. was supported by NRF of Korea (Grant No. 2017R1A5A1014862, SRC program: vdWMRC center) and KIAS individual Grant (No. CG031509). Computations were supported by the CAC of KIAS.

*Present address: Theoretical Division, Los Alamos National Laboratory, Los Alamos, New Mexico 87545, USA.
†garix.minjae.kim@gmail.com
‡hand@kias.re.kr

[1] E. Verwey, Electronic conduction of magnetite (Fe_3O_4) and its transition point at low temperatures, Nature (London) **144**, 327 (1939).

[2] Y. Yamada, O. Hino, S. Nohdo, R. Kanao, T. Inami, and S. Katano, Polaron Ordering in Low-Doping $La_{1-x}Sr_xMnO_3$, Phys. Rev. Lett. **77**, 904 (1996).

[3] B. B. Van Aken, O. D. Jurchescu, A. Meetsma, Y. Tomioka, Y. Tokura, and T. T. M. Palstra, Orbital-Order-Induced Metal-Insulator Transition in $La_{1-x}Ca_xMnO_3$, Phys. Rev. Lett. **90**, 066403 (2003).

[4] J. Tranquada, B. Sternlieb, J. Axe, Y. Nakamura, and S. Uchida, Evidence for stripe correlations of spins and holes in copper oxide superconductors, Nature (London) **375**, 561 (1995).

[5] E. H. da Silva Neto, P. Aynajian, A. Frano, R. Comin, E. Schierle, E. Weschke, A. Gyenis, J. Wen, J. Schneeloch, Z. Xu, S. Ono, G. Gu, M. L. Tacon, and A. Yazdani, Ubiquitous interplay between charge ordering and high-temperature superconductivity in cuprates, Science **343**, 393 (2014).

[6] E. H. da Silva Neto, R. Comin, F. He, R. Sutarto, Y. Jiang, R. L. Greene, G. A. Sawatzky, and A. Damascelli, Charge ordering in the electron-doped superconductor $Nd_{2-x}Ce_xCuO_4$, Science **347**, 282 (2015).

[7] A. Frano, S. Blanco-Canosa, B. Keimer, and R. J. Birgeneau, Charge ordering in superconducting copper oxides, J. Phys. Condens. Matter **32**, 374005 (2020).

[8] L. Mattheiss, E. M. Gyorgy, and D. W. Johnson Jr, Superconductivity above 20 K in the Ba-K-Bi-O system, Phys. Rev. B **37**, 3745 (1988).

[9] R. J. Cava, B. Batlogg, J. J. Krajewski, R. Farrow, L. W. Rupp, A. E. White, K. Short, W. F. Peck, and T. Kometani, Superconductivity near 30 K without copper: The $Ba_{0.6}K_{0.4}BiO_3$ perovskite, Nature (London) **332**, 814 (1988).

[10] A. Ramirez, Colossal magnetoresistance, J. Phys. Condens. Matter **9**, 8171 (1997).

[11] J. Van Den Brink and D. I. Khomskii, Multiferroicity due to charge ordering, J. Phys. Condens. Matter **20**, 434217 (2008).

[12] J. P. Attfield, Charge ordering in transition metal oxides, Solid State Sci. **8**, 861 (2006).

[13] W. Kohn and L. J. Sham, Self-consistent equations including exchange and correlation effects, Phys. Rev. **140**, A1133 (1965).

[14] J. P. Perdew, J. A. Chevary, S. H. Vosko, K. A. Jackson, M. R. Pederson, D. J. Singh, and C. Fiolhais, Atoms, molecules, solids, and surfaces: Applications of the generalized gradient approximation for exchange and correlation, Phys. Rev. B **46**, 6671 (1992).

[15] V. Anisimov, I. Elfimov, N. Hamada, and K. Terakura, Charge-ordered insulating state of Fe_3O_4 from first-principles electronic structure calculations, Phys. Rev. B **54**, 4387 (1996).

[16] T. Tsumuraya, H. Seo, and T. Miyazaki, First-principles study of the charge ordered phase in $\kappa - D_3(\text{Cat-EDT-TTF/ST})_2$: Stability of π-electron deuterium coupled ordering in hydrogen-bonded molecular conductors, Phys. Rev. B **101**, 045114 (2020).

[17] J. Hubbard, Electron correlations in narrow energy bands, Proc. R. Soc. A **276**, 238 (1963).

[18] M. Schüler, M. Rösner, T. O. Wehling, A. I. Lichtenstein, and M. I. Katsnelson, Optimal Hubbard Models for Materials with Nonlocal Coulomb Interactions: Graphene, Silicene, and Benzene, Phys. Rev. Lett. **111**, 036601 (2013).

[19] H. Seo, Charge ordering in organic ET compounds, J. Phys. Soc. Jpn. **69**, 805 (2000).

[20] S. Yamamoto, T. Fujiwara, and Y. Hatsugai, Electronic structure of charge and spin stripe order in $La_{2-x}Sr_xNiO_4$ ($x = \frac{1}{3}, \frac{1}{2}$), Phys. Rev. B **76**, 165114 (2007).

[21] H. Terletska, T. Chen, and E. Gull, Charge ordering and correlation effects in the extended Hubbard model, Phys. Rev. B **95**, 115149 (2017).

[22] D. Cox and A. Sleight, Crystal structure of $Ba_2Bi^{3+}Bi^{5+}O_6$, Solid State Commun. **19**, 969 (1976).

[23] D. E. Cox and A. W. Sleight, Mixed-valent $Ba_2Bi^{3+}Bi^{5+}O_6$: Structure and properties, Acta Crystallogr. Sect. B **35**, 1 (1979).

[24] M. Kim, G. M. McNally, H.-H. Kim, M. Oudah, A. S. Gibbs, P. Manuel, R. J. Green, R. Sutarto, T. Takayama, A. Yaresko, U. Wedig, M. Isobe, R. K. Kremer, D. A. Bonn, B. Keimer, and H. Takagi, Superconductivity in $(Ba,K)SbO_3$, Nat. Mater. **21**, 627 (2022).

[25] A. I. Liechtenstein, I. I. Mazin, C. O. Rodriguez, O. Jepsen, O. K. Andersen, and M. Methfessel, Structural phase diagram and electron-phonon interaction in $Ba_{1-x}K_xBiO_3$, Phys. Rev. B **44**, 5388 (1991).

[26] V. Meregalli and S. Y. Savrasov, Electron-phonon coupling and properties of doped $BaBiO_3$, Phys. Rev. B **57**, 14453 (1998).

[27] V. Meregalli and S. Y. Savrasov, Electron-phonon coupling and properties of doped $BaBiO_3$, J. Supercond. Nov. Magn. **12**, 185 (1999).

[28] T. Thonhauser and K. M. Rabe, Fcc breathing instability in $BaBiO_3$ from first principles, Phys. Rev. B **73**, 212106 (2006).

[29] D. Korotin, V. Kukolev, A. V. Kozhevnikov, D. Novoselov, and V. I. Anisimov, Electronic correlations and crystal structure distortions in $BaBiO_3$, J. Phys. Condens. Matter **24**, 415603 (2012).

[30] D. M. Korotin, D. Novoselov, and V. I. Anisimov, Correlation effects and phonon modes softening with doping in $Ba_{1-x}K_xBiO_3$, J. Phys. Condens. Matter **26**, 195602 (2014).

[31] C. Franchini, A. Sanna, M. Marsman, and G. Kresse, Structural, vibrational, and quasiparticle properties of the Peierls semiconductor $BaBiO_3$: A hybrid functional and self-consistent GW+vertex-corrections study, Phys. Rev. B **81**, 085213 (2010).

[32] C. Franchini, G. Kresse, and R. Podloucky, Polaronic Hole Trapping in Doped $BaBiO_3$, Phys. Rev. Lett. **102**, 256402 (2009).

[33] Z. P. Yin, A. Kutepov, and G. Kotliar, Correlation-Enhanced Electron-Phonon Coupling: Applications of GW and Screened Hybrid Functional to Bismuthates, Chloronitrides, and Other High-Tc Superconductors, Phys. Rev. X **3**, 021011 (2013).

[34] Z. Li, G. Antonius, M. Wu, F. H. da Jornada, and S. G. Louie, Electron-Phonon Coupling from *Ab Initio* Linear-Response Theory within the GW Method: Correlation-Enhanced Interactions and Superconductivity in $Ba_{1-x}K_xBiO_3$, Phys. Rev. Lett. **122**, 186402 (2019).

[35] Z. Yuan, P. Zheng, Y. Peng, R. Liu, X. Ma, G. Wang, T. Yu, and Z. Yin, Correlation-enhanced electron-phonon coupling and superconductivity in (Ba, K)SbO_3 superconductors, Phys. Rev. B **105**, 014517 (2022).

[36] L. A. Agapito, S. Curtarolo, and M. Buongiorno Nardelli, Reformulation of DFT + U as a Pseudohybrid Hubbard Density Functional for Accelerated Materials Discovery, Phys. Rev. X **5**, 011006 (2015).

[37] N. Tancogne-Dejean, M. A. Sentef, and A. Rubio, Ultrafast Modification of Hubbard U in a Strongly Correlated Material: *Ab initio* High-Harmonic Generation in NiO, Phys. Rev. Lett. **121**, 097402 (2018).

[38] S.-H. Lee and Y.-W. Son, First-principles approach with a pseudohybrid density functional for extended hubbard interactions, Phys. Rev. Res. **2**, 043410 (2020).

[39] N. Tancogne-Dejean and A. Rubio, Parameter-free hybrid-like functional based on an extended Hubbard model: DFT + U + V, Phys. Rev. B **102**, 155117 (2020).

[40] V. L. Campo Jr and M. Cococcioni, Extended DFT + U + V method with on-site and inter-site electronic interactions, J. Phys. Condens. Matter **22**, 055602 (2010).

[41] J. Huang, S.-H. Lee, Y.-W. Son, A. Supka, and S. Liu, First-principles study of two-dimensional ferroelectrics using self-consistent Hubbard parameters, Phys. Rev. B **102**, 165157 (2020).

[42] H. J. Kulik and N. Marzari, Transition-metal dioxides: A case for the intersite term in hubbard-model functionals, J. Chem. Phys. **134**, 094103 (2011).

[43] M. Cococcioni and N. Marzari, Energetics and cathode voltages of Li$M$$PO_4$ olivines (M = Fe, Mn) from extended Hubbard functionals, Phys. Rev. Mater. **3**, 033801 (2019).

[44] C. Ricca, I. Timrov, M. Cococcioni, N. Marzari, and U. Aschauer, Self-consistent DFT + U + V study of oxygen vacancies in $SrTiO_3$, Phys. Rev. Res. **2**, 023313 (2020).

[45] I. Timrov, F. Aquilante, L. Binci, M. Cococcioni, and N. Marzari, Pulay forces in density-functional theory with extended Hubbard functionals: From nonorthogonalized to orthogonalized manifolds, Phys. Rev. B **102**, 235159 (2020).

[46] W. Yang, S.-H. Jhi, S.-H. Lee, and Y.-W. Son, *Ab initio* study of lattice dynamics of group IV semiconductors using pseudohybrid functionals for extended Hubbard interactions, Phys. Rev. B **104**, 104313 (2021).

[47] I. Timrov, N. Marzari, and M. Cococcioni, Self-consistent hubbard parameters from density-functional perturbation theory in the ultrasoft and projector-augmented wave formulations, Phys. Rev. B **103**, 045141 (2021).

[48] I. Timrov, F. Aquilante, M. Cococcioni, and N. Marzari, Accurate electronic properties and intercalation voltages of olivine-type Li-ion cathode materials from extended hubbard functionals, PRX Energy **1**, 033003 (2022).

[49] W. Yang, B. G. Jang, Y.-W. Son, and S.-H. Jhi, Lattice dynamical properties of antiferromagnetic oxides calculated using self-consistent extended hubbard functional method, J. Phys. Condens. Matter **34**, 295601 (2022).

[50] See Supplemental Materials at http://link.aps.org/supplemental/10.1103/PhysRevLett.130.136401 for detailed computational methods, comprehensive phonon dispersions, and self-consistent extended Hubbard parameters, which includes Refs. [51–55].

[51] N. J. Mosey and E. A. Carter, *Ab initio* evaluation of coulomb and exchange parameters for DFT + U calculations, Phys. Rev. B **76**, 155123 (2007).

[52] N. J. Mosey, P. Liao, and E. A. Carter, Rotationally invariant *ab initio* evaluation of coulomb and exchange parameters for DFT + U calculations, J. Chem. Phys. **129**, 014103 (2008).

[53] P. Giannozzi, S. Baroni, N. Bonini, M. Calandra, R. Car, C. Cavazzoni, D. Ceresoli, G. L. Chiarotti, M. Cococcioni, I. Dabo *et al.*, QUANTUM ESPRESSO: A modular and open-source software project for quantum simulations of materials, J. Phys. Condens. Matter **21**, 395502 (2009).

[54] M. J. van Setten, M. Giantomassi, E. Bousquet, M. J. Verstraete, D. R. Hamann, X. Gonze, and G.-M. Rignanese, The PseudoDojo: Training and grading a 85 element optimized norm-conserving pseudopotential table, Comput. Phys. Commun. **226**, 39 (2018).

[55] G. Kim, M. Neumann, M. Kim, M. D. Le, T. D. Kang, and T. W. Noh, Suppression of Three-Dimensional Charge Density Wave Ordering via Thickness Control, Phys. Rev. Lett. **115**, 226402 (2015).

[56] S. Pei, J. D. Jorgensen, B. Dabrowski, D. G. Hinks, D. R. Richards, A. W. Mitchell, J. M. Newsam, S. K. Sinha, D. Vaknin, and A. J. Jacobson, Structural phase diagram of the $Ba_{1-x}K_xBiO_3$, Phys. Rev. B **41**, 4126 (1990).

[57] B. J. Kennedy, C. J. Howard, K. S. Knight, Z. Zhang, and Q. Zhou, Structures and phase transitions in the ordered double perovskites $Ba_2Bi^{III}Bi^{V}O_6$ and $Ba_2Bi^{III}Sb^{V}O_6$, Acta Crystallogr. Sect. B **62**, 537 (2006).

[58] N. C. Plumb, D. J. Gawryluk, Y. Wang, Z. Ristić, J. Park, B. Q. Lv, Z. Wang, C. E. Matt, N. Xu, T. Shang, K. Conder, J. Mesot, S. Johnston, M. Shi, and M. Radović, Momentum-Resolved Electronic Structure of the High-Tc Superconductor Parent Compound $BaBiO_3$, Phys. Rev. Lett. **117**, 037002 (2016).

[59] J. S. Oh, M. Kim, G. Kim, H. G. Lee, H. K. Yoo, S. Sinn, Y. J. Chang, M. Han, C. Jozwiak, A. Bostwick, E. Rotenberg, H. D. Kim, and T. W. Noh, Evidence for absence of metallic surface states in BiO2-terminated BaBiO3 thin films, Curr. Appl. Phys. **18**, 658 (2018).

[60] A. Togo and I. Tanaka, First principles phonon calculations in materials science, Scr. Mater. **108**, 1 (2015).

[61] M. Braden, W. Reichardt, W. Schmidbauer, A. S. Ivanov, and A. Y. Rumiantsev, Lattice dynamics of (Ba/K)BiO_3, J. Supercond. **8**, 595 (1995).

[62] C. K. Loong, P. Vashishta, R. K. Kalia, W. Jin, M. H. Degani, D. G. Hinks, D. L. Price, J. D. Jorgensen, B. Dabrowski, A. W. Mitchell, D. R. Richards, and Y. Zheng, Phonon density of states and oxygen-isotope effect in $Ba_{1-x}K_xBiO_3$, Phys. Rev. B **45**, 8052 (1992).

[63] M. Braden, W. Reichardt, A. S. Ivanov, and A. Y. Rumiantsev, Anomalous dispersion of LO phonon branches in $Ba_{0.6}K_{0.4}BiO_3$, Europhys. Lett. **34**, 531 (1996).

[64] M. Braden, W. Reichardt, S. Shiryaev, and S. N. Barilo, Giant phonon anomalies in the bond-stretching modes in doped $BaBiO_3$: Comparison to cuprates manganites and nickelates, Phys. C Supercond. Appl. **378**, 89 (2002).

[65] S. Tajima, M. Yoshida, N. Koshizuka, H. Sato, and S. Uchida, Raman-scattering study of the metal-insulator transition in $Ba_{1-x}K_xBiO_3$, Phys. Rev. B **46**, 1232 (1992).

[66] M. Braden, W. Reichardt, E. Elkaim, J. P. Lauriat, S. Shiryaev, and S. N. Barilo, Structural distortion in superconducting $Ba_{1-x}K_xBiO_3$, Phys. Rev. B **62**, 6708 (2000).

[67] R. M. Fleming, P. Marsh, R. J. Cava, and J. J. Krajewski, Temperature dependence of the lattice parameters in the 30-K superconductor $Ba_{0.6}K_{0.4}BiO_3$, Phys. Rev. B **38**, 7026 (1988).

[68] C.-J. Kang and G. Kotliar, Material design of indium-based compounds: Possible candidates for charge, valence, and bond disproportionation and superconductivity, Phys. Rev. Mater. **3**, 015001 (2019).